A modified thermal wall function for the estimation of gas-to-wall heat fluxes in CFD in-cylinder simulations of high performance spark-ignition engines

Fabio Berni[a], Giuseppe Cicalese[a], Stefano Fontanesi[a]
[a]University of Modena and Reggio Emilia
Department of Engineering "Enzo Ferrari", via P. Vivarelli 10, 41125, Modena
Corresponding author: Fabio Berni, tel. +39 059 2058781 – fax +39 059 2056126 – email fabio.berni@unimore.it

KEYWORDS
Heat transfer, engine thermal survey, law of the wall, thermal wall function, conjugate heat transfer, CFD

Abstract

Last generation spark ignition (SI) engines are characterized by a simultaneous reduction of the engine displacement and an increase of the brake power; such conflicting targets are achieved through the adoption of several techniques such as turbocharging, direct fuel injection, variable valve timing and variable port lengths. This design approach, referred to as "engine downsizing", leads to a remarkable increase in the thermal loads acting on the engine components facing the combustion chamber. Hence, an accurate evaluation of the thermal field is of primary importance in order to avoid thermo-mechanical failures. Moreover, the correct evaluation of the temperature distribution improves the prediction of point-wise abnormal combustion onset.

Due to the complexity of the experimental measurement of instantaneous gas-to-wall heat fluxes, 3D-CFD simulations of the in-cylinder processes are a fundamental tool to evaluate not only the global amount of heat transferred to the combustion chamber walls, but also its point-wise distribution. Several heat transfer models and thermal laws of the wall are available in literature, most of which were developed in the past decades and calibrated against experiments carried out in research laboratories at relatively low-load / low-speed engine operations. In the present paper two widely adopted heat transfer models are proved to be effective at such conditions to predict gas-to-wall heat flux, as demonstrated by their application to the well-known GM pancake engine test case. However, despite such comforting results, they manifest evident shortages when used for highly-charged / highly-downsized current production SI engines, since operated at specific thermal loads and engine speeds very different from the above experiments. In particular, overestimations of the wall heat transfer predicted by such thermal laws of the wall are pointed out thanks to experimental engine thermal surveys and temperature measurements on four current production engines.

Therefore an alternative heat transfer model is proposed by the authors and tested on such currently made turbocharged SI engines, operated at different conditions. Compared to the existing models differences are pointed out, especially in terms of law of the wall expression. Experimental engine thermal survey and point-wise temperature measurements are used to validate the numerical heat flux. In particular the increased predictive capabilities of the 3D-CFD gas-to-wall heat transfer simulations are revealed both in terms of global thermal balance and temperature distribution of the metal for all the investigated engines. In fact model adoption in a combined in-cylinder / CHT (Conjugate Heat Transfer) simulation loop leads to a correct characterization of the thermal status of all the analyzed engines. Finally, alternative model adoption for the investigated current production high specific power DISI turbocharged engines operated at full load and high revving speed is critically motivated adopting the "isothermicity parameter" ζ which represents an indication of the thermal state of the boundary layer, being a characteristic scale of the ratio between gas and wall temperatures.

1. Introduction

New generation of internal combustion SI engines is characterized by high specific power. This is a consequence of more and more stringent laws that push engine manufacturers to lower fuel consumption and pollutant emissions. In order to meet such targets, automotive industry relies on several techniques such as turbocharging, engine downsizing and down-speeding, complex fuel injection strategies, variable valve timing, variable port length [1,2], innovative combustion modes (e.g. RCCI) and water a/o methanol injection [3,4]. Moreover, the possibility to hybridize vehicles cannot be neglected, which is an increasingly widespread solution. However, the increase of specific power thanks to downsizing and turbocharging is limited on one hand by the occurrence of abnormal combustions [5], on the other hand by the risk of thermo-mechanical failures. The raise of the thermal loads can significantly reduce the mechanical resistance of the engine components thus deeply reducing the engine reliability [6]. In order to avoid knock onset, the most diffused solution is the reduction of the engine spark advance (SA), thus lowering the engine performance.

In order to prevent thermo-mechanical damages, CFD-CHT and FE tools may be used to calculate the thermal field and thermo-mechanical stresses of the engine, reducing proficiently time- and cost-to market. For this purpose it is fundamental to estimate correctly the gas-to-wall heat transfer, which affects not only the thermal stresses, but also the overall engine efficiency and the exhaust emissions. As highlighted by Nijeweme et al. [7] the formation rate of NO_x is strictly dependent on temperature and a reduction of about 30 K in the peak combustion temperature can halve the NO_x emissions. Also wall temperatures are found to be important for emissions. In fact, Alkidas and Myers [8] show that, on one hand, NO_x emissions increase strongly with surface temperatures, on the other hand HC emissions decrease when coolant temperature raises. Furthermore, wall heat transfer should be correctly predicted to improve the accuracy of in-cylinder simulations, as it affects charge mixing and combustion.

A correct estimate of the gas-to-wall thermal loads is fundamental and it can be derived from either dedicated experiments or 1D/3D CFD simulations. The thermal power acting on the components facing the combustion chamber cannot be experimentally assessed without efforts. In fact,

a direct evaluation of the instantaneous heat flux usually requires the adoption of complex, expensive and intrusive sensors [9,10], which cannot be used for moving parts (e.g. piston and valves). Otherwise, thanks to recent technological developments, particular thermocouples can be used to measure surface temperatures on engine components, even on the moving ones. Such fast response thermocouples, called Thin Film Gauges (TFG), can be placed on the valve face or even on the piston crown [11] to measure local surface temperatures which, once processed, can provide local heat fluxes. Unfortunately, using this kind of instruments two problems arise at least. First of all, to the extent of the authors' knowledge, measurements have been performed only at operating conditions far from the peak power ones of current production SI turbocharged engines. Secondly, surface temperature measurements are not sufficient to estimate the heat flux. In order to solve the heat conduction equation a second condition has to be found. In [7,9,10] such condition, which allows to estimate the steady-state component of the heat flux, is given by a reference thermocouple immersed in the probe containing the surface thermocouple. This reference thermocouple is located at a known distance from the wall, where the temperature fluctuations have reasonably decayed. In other words, at that depth, temperature is constant and does not change during the engine cycle because of the heat capacity of the component. So in [7,9,10] duplex thermocouples are used. When TFG are used, the reference measurements is missing, so the estimation of the heat flux is based on a partially erroneous hypothesis as in [11], that is the heat flux is supposed to be null when the gas temperature equals the wall temperature. Nijeweme et al. in [7] investigate deeply the in-cylinder heat transfer from both a numerical and an experimental point of view. Thanks to a duplex thermocouple, experimental wall heat fluxes are estimated correctly and are proved not to be null when gas and wall temperatures are equal. Also Lawton in [12] points out that even if the temperature difference is zero, there is a positive heat flux during compression and a negative one during expansion.

Regardless the method, measurements can be performed only in limited portions of the components, and the resulting total thermal power due to combustion has to be extrapolated in both space and time. As a consequence, engine manufacturers prefer to rely on their own experience (derived from similar engines) or, more often, on indirect methods. Such methods consist of a thermal load estimation by means of a thermal survey of the engine: test bench experiments allow to measure all the contributions included in the engine thermal balance (such as heat to lubricant, heat to coolant, brake power, etc.) and thus to quantify the global amount of thermal power acting on the engine components. In addition, during such tests, thermocouples are often placed in the most critical locations in order to evaluate engine temperature pointwise distributions. Once the global amount is estimated, it is split among each component (for example head, liner and piston) thanks to a combination of experimental evidence and user experience. It can be finally used in CFD-CHT and FE tools to calculate the thermal field of the engine. A good agreement between the simulated thermal field and the experimental one (measured by thermocouples) is used to attest the simulation success. It is worthwhile to highlight that such kind of approach relies on significant approximations, e.g. the global thermal load split between all the components and its spatial distribution on each of them, which can be either constant in space or spread on the basis of physical assumptions and experimental evidences.

For many decades experimental measurements, focused on in-cylinder heat transfer, have been published by many researchers both in CI and SI reciprocating engines. Annand [13] and Woschni [14] were the first to test Diesel engines, while as for spark-ignition engines Alkidas' experimental campaign [9] has to be mentioned. Besides experimental studies, in the last years the attention of industry and research is more and more focused on simulation models which are becoming an essential support for automotive design. Many mathematical formulations have been proposed aiming to estimate reliably heat transfer through the combustion chamber walls. As Rakopoulos suggests in [15], two major groups of heat transfer models can be identified: the phenomenological and the CFD ones. As for the former, empirical formulations are proposed which aim to be universally applicable. Unfortunately, as Woschni himself admits in [14] commenting his correlation, the universal validity of the formula should be expected only if new constants were adopted when engine design varies. In other words the constants, to be experimentally determined, can be maintained only for geometrically similar engines, otherwise they have to be tuned. This is due to the relative simplicity of such formulations. As for the latter, proposed formulations rely on a deeper investigation of the heat transfer mechanism, thus providing more robust estimation of the heat fluxes. However, the major challenge of such models is to limit the computational effort without loss of accuracy. In fact, as highlighted by Nuutinen [16], in commercial CFD software there are two kinds of approach for the modeling of the convective heat transfer in a RANS framework. In the first one a wall function with a high-Reynolds number turbulence model can be applied, avoiding to increase (for computational cost reasons) the number of near–wall cells to capture accurately the flow and the heat transfer in the proximity of the walls. In the second one a refined computational grid with a low-Reynolds number or a two-layer turbulence model is adopted, to resolve spatially the near-wall profiles of velocity and temperature. Despite the high resolution of such approach, which should provide the most accurate results, it often leads to prohibitive computational costs. Therefore, the adoption of an analytical wall function is still the most common solution among the CFD approaches, since it provides more reliable heat flux estimations if compared to the phenomenological heat transfer models.

In order to reduce assumptions and uncertainties in the estimation of the amount and pointwise distribution of the thermal loads acting on the engine components, CFD tools may replace experimental measurements. Investigations by the authors [17-21] show that the integration between 3D-CFD in-cylinder simulations and CHT ones provides a very accurate representation of the engine thermal field, which can be used, coupled with FE tools, to fix design issues that may lead to abnormal combustions or thermo-mechanical failures. In such interaction, a fundamental role is played by the capability of the CFD in-cylinder model to estimate accurately the wall heat flux due to combustion, which in turn depends strongly on the thermal wall function. Researchers have proposed formulations for years, aiming at capturing the actual heat flux through the combustion chamber boundaries. Despite the huge number of thermal wall functions that can be found in literature (among which the most used will be revised later on), none seems to be suitable for all the engine applications: CI and SI engines, low and high revving speeds, partial and full loads.

Given the above the authors intend to propose, in the present paper, a wall heat transfer model to be used in in-cylinder simulations of current production high performance spark-ignition engines operated at medium-to-high loads and revving speeds, in order to obtain reliable convective heat fluxes acting on the engine components. The predictive capability of the simulated wall heat transfer is proved twice: on one hand the calculated global amount of wall heat flux is compared with the experimental one provided by the engine thermal survey. On the other hand the simulated thermal field (provided by the CHT simulation, which in turn depends on the wall heat fluxes) is compared with the experimental one resulting from thermocouple measurements.

In the following paragraphs the paper offers an overview of the analyzed engines and the experimental data. Subsequently a brief review of the most adopted heat transfer models is reported and a modified wall function is proposed by the authors. Afterwards the numerical set-up is described and

preliminary outcomes are shown. Finally, the results relative to the application of the proposed model are presented and discussed and conclusions are drawn.

2. Experimental Measurements

2.1 Engine Overview

Four currently produced direct injection spark ignition (DISI) turbocharged engines are investigated in the current paper. For the sake of confidentiality they are referred to as Engine A, B, C and D. Some of the main engine characteristics are reported in Table 1. Engine A is analyzed at two different operating conditions: 7000 rpm WOT (peak power, here after referred to as Operating Condition 1) and 5000 rpm WOT (peak torque, here after referred to as Operating Condition 2). Engine B, C and D are investigated only at the peak power condition, respectively 7000rpm WOT, 5200rpm WOT and 6000rpm WOT.

Engine A – Op.Cond.1		Engine A – Op.Cond.2		Engine B		Engine C		Engine D	
B/S	1.05	B/S	1.05	B/S	1.04	B/S	0.93	B/S	0.93
Revving Speed	7000 rpm	Revving Speed	5000 rpm	Revving Speed	7000 rpm	Revving Speed	5200 rpm	Revving Speed	6000 rpm
BMEP	18.3 bar	BMEP	24.4 bar	BMEP	23.3 bar	BMEP	22.9 bar	BMEP	30.4 bar

Table 1. Engine features and operating conditions

2.2 Engine Thermal Survey

Engines operated at a fixed condition can be studied as a steady-state system where energy enters and exits. The combustion process converts the chemical energy of the fuel into thermal energy, which in turn transforms partially into indicated work. The remaining part heats up the lubricating and the coolant circuits, increases the exhaust gas enthalpy and is lost to the ambient. The main goal of an experimental engine thermal survey is the analysis of such thermal power subdivision, to estimate how much of the heat due to combustion and friction is managed and removed by both the coolant and the lubricating circuits.

Even if detrimental for the efficiency, the coolant circuit is necessary to remove heat from the engine components and hence to limit their temperature. Also the oil circuit concurs to engine cooling, besides guaranteeing an adequate lubrication of the components. In particular, lubricating circuit cools down pistons by means of oil jets and removes heat due to frictions. Typical coolant and lubricating circuit layouts of the investigated engines are schematically shown in Figure 1.

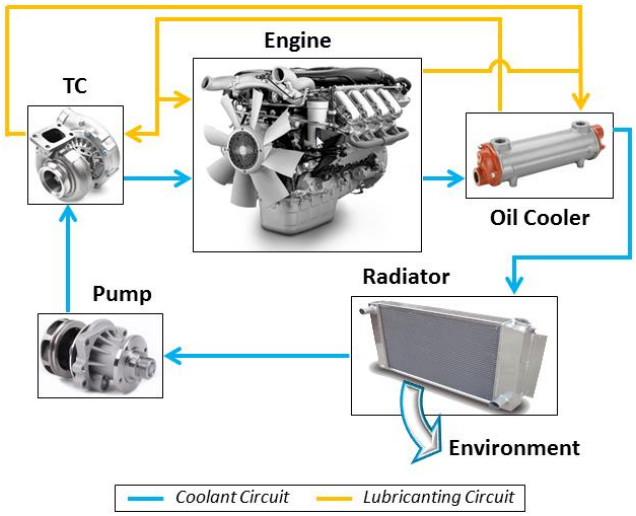

Figure 1. Simplified coolant circuit layout

After passing through the turbocharger, the coolant enters the engine and then cools down the lubricant by means of the oil cooler. Finally, a liquid-to-air heat exchanger (the radiator) allows the thermal power to be released to the environment. As for the oil, it cools simultaneously engine and turbochargers before being cooled in a liquid-to-liquid exchanger (oil cooler).

Both for the coolant and the lubricating circuit, the heat removed from each component of the circuit by the liquid can be estimated if mass flow rate, specific heat and temperature drop across the component are known or measured. In the experiments carried out on the analyzed engines, the temperature drop was measured by means of purposely placed temperature sensors (RTD) at the inlet and outlet of each element. At least two probes were adopted in any measurement section of the circuit to avert poor-mixing problems of the fluid. Also mass flow rates were measured by means of

precise Coriolis flow meters and the specific heat was known both for the coolant and the lubricant. Hence the heat ($\dot{Q}_{coolant}$) removed by the coolant passing through the engine galleries can be identified thanks to data provided by the experimental tests.

It should be noted that such portion of the coolant circuit pertaining to the engine (i.e. block and head galleries) is included in the CHT computational domain, whose components are accurately described in CHT Model section. Hence the numerical $\dot{Q}_{coolant}$ provided by the CHT simulation has to match the experimental counterpart. Since the coolant circuit surrounds the combustion chamber removing the largest amount of the gas-to-wall heat flux, basically only $\dot{Q}_{coolant}$ is strongly affected by $\dot{Q}_{comb}$, which is a thermal power entering the CHT domain and due to the heat transfer occurring among hot gases and combustion chamber walls. In fact all other terms appearing on the right side of the CHT domain thermal balance shown in Figure 2 and described by equation (1) are at least one order of magnitude lower. Such terms are the thermal power ($\dot{Q}_{env}$) lost to the environment and the one removed by the lubricating circuit ($\dot{Q}_{lubr}$). On the left side of the equation (1) also $\dot{Q}_{fric}$ and $\dot{Q}_{surr}$ are one order of magnitude lower than $\dot{Q}_{comb}$. These are thermal powers entering the domain and due respectively to frictions and surrounding components. $\dot{Q}_{fric}$ is generated by frictions between pistons and liners and between crankshaft, camshaft and their respective bearings. Finally $\dot{Q}_{surr}$ is due to heat conduction from surrounding components such as the exhaust manifold, which heats up the exhaust flange present in the computational domain. Both $\dot{Q}_{fric}$ and $\dot{Q}_{surr}$ are adopted in the CHT model as boundary conditions. Therefore if numerical $\dot{Q}_{coolant}$ does not match the experimental one, the major responsible is $\dot{Q}_{comb}$.

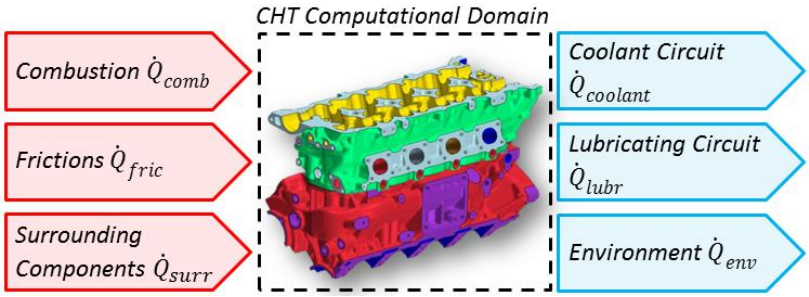

$$\dot{Q}_{comb} + \dot{Q}_{fric} + \dot{Q}_{surr} = \dot{Q}_{coolant} + \dot{Q}_{lubr} + \dot{Q}_{env} \qquad (1)$$

Figure 2. CHT computational domain thermal power balance

Simultaneously, since $\dot{Q}_{coolant}$ is known from tests, following equation (1) an experimental target can be obtained for $\dot{Q}_{comb}$. In fact $\dot{Q}_{fric}$ is separately assessed based on the operating conditions (revving speed and load) which affect the in-cylinder pressure and piston velocity. $\dot{Q}_{surr}$ is estimated starting from experimental evidences such as the exhaust gas and exhaust manifold temperatures. As for $\dot{Q}_{lubr}$ and $\dot{Q}_{env}$, they are extracted from the CHT simulations and they depend on the heat transfer coefficients and reference temperatures imposed at the CHT domain boundaries facing the lubricant circuit and the environment. In particular a numerical heat flux ($\dot{Q}_{comb}$) calculated by means of a dedicated in-cylinder simulation is imposed to the CHT model and scaled in order to obtain a numerical $\dot{Q}_{coolant}$ matching the experimental one. The $\dot{Q}_{lubr}$ and $\dot{Q}_{env}$ resulting from CHT simulation along with the imposed $\dot{Q}_{fric}$ and $\dot{Q}_{surr}$ and the experimental $\dot{Q}_{coolant}$ allow to obtain an experimental target for $\dot{Q}_{comb}$ which corresponds obviously to the scaled heat flux applied to the CHT model. The obtained heat flux targets for all the analyzed engines are reported in Table 2.

	Engine A 7000 rpm	**Engine A 5000 rpm**	**Engine B**	**Engine C**	**Engine D**
	kW	**kW**	**kW**	**kW**	**kW**
Cylinder Target	13.6 ± 4.1	10.3 ± 3.1	14.1 ± 4.2	9.12 ± 2.7	11.7 ± 3.5

Table 2. Target heat transfer of a single cylinder, for each analyzed engine

It is evident that such targets are not completely experimentally determined unless $\dot{Q}_{fric}$, $\dot{Q}_{surr}$, $\dot{Q}_{lubr}$ and $\dot{Q}_{env}$ are known from tests. Luckily, as stated before, $\dot{Q}_{fric}$, $\dot{Q}_{surr}$, $\dot{Q}_{lubr}$ and $\dot{Q}_{env}$ are at least one order of magnitude lower than $\dot{Q}_{comb}$ and $\dot{Q}_{coolant}$. Therefore, even if these quantities are not experimentally assessed (as a matter of fact only $\dot{Q}_{coolant}$ comes from tests), their impact on the $\dot{Q}_{comb}$ target estimation is pretty restrained. The uncertainties in such estimations as well as experimental measurement errors for $\dot{Q}_{coolant}$ are accounted for in the uncertainties (equal to 30%) reported in Table 2.

Hence, collecting data deriving from experimental thermal survey (performed for each analyzed engine a/o operating condition) and CHT simulations, equation (1) can provide a target global wall heat flux. In other words, global heat transfer due to combustion and acting on the walls facing the hot gases can be obtained from the engine thermal balance depicted in Figure 2 and described by equation (1). It should be noted that "global" stands for the sum of the fluxes pertaining to each cylinder. In order to obtain the target heat flux of a single cylinder (as reported in Table 2), identical combustions are assumed for the different cylinders, so that the global amount could be simply divided by the cylinder number.

Once the target is known, numerical instantaneous heat flux provided by any in-cylinder wall heat transfer model can be cycle-averaged and then compared to such target in order to validate the thermal wall function. In other words, the obtained cylinder target can be used to identify which heat transfer model is able to estimate properly the heat flux acting on the components facing the combustion chamber.

2.3 Thermocouple Measures

The global thermal load due to combustion is not the only experimental information that can be obtained from tests. Frequently in fact, during experimental thermal surveys, thermocouples are placed within the engine to measure wall temperatures. In this case, for each investigated engine (except unit B), a relevant number of thermocouples was placed at the most critical locations of the engine block and head (such as at the junction of the exhaust ports for each cylinder, at the portion of flame deck among the exhaust valves or even along the liners in different angular positions). The goal is to monitor temperatures in such critical locations in order to ensure they do not reach excessive values for the sake of thermo-mechanical resistance. Therefore, a second numerical-experimental comparison can be carried out in order to validate the heat transfer model. In particular, numerical temperatures evaluated by means of probes located in the CHT model at the same positions as the experimental thermocouples can be compared to the experimental ones. Numerical heat fluxes can be considered calculated accurately only if enabling to match both the experimental thermal survey and the temperature field.

3. 3D-CFD Wall Heat Transfer Modeling

3.1 Existing Models

As stated in the introduction, many researchers attempted to propose heat transfer models (even universal) for CFD in-cylinder simulations. Starting from the evidence that turbulent flows exhibit universal velocity and temperature near-wall profiles if wall distance, velocity and temperature are properly scaled, the first models were developed for isothermal or nearly-isothermal flows. Among the most widespread heat transfer models for isothermal flows, Launder and Spalding [22] proposed a model based on a viscous sublayer resistance factor according to the experiments conducted by Jayatillake [23]. Also Kays and Crawford [24] developed a formulation starting from the energy differential equation of the boundary layer. Simplifying the equation and restricting considerations to air, they obtained their own algebraic closed-form solution, as shown in Appendix. Huh et Al. [25], compared to Kays and Crawford's heat transfer model, tried to include the effect of the so called "work term", that is the pressure derivative over time. Such rate of pressure rise term was identified as the responsible for significant effects on engine heat transfer, such as the inversion of the heat flux, which may be directed from the wall to the gas even if the second one is hotter. The importance of such unsteady term was highlighted also by Nijeweme et Al. [7]. They compared the heat fluxes obtained by means of a "traditional" wall function (similar to the Launder and Spalding one) with experimental heat fluxes and with the results provided by a complete modeling of the unsteady flow and heat conduction within the boundary layer. They were able to conclude that a reliable estimation of the heat fluxes by means of CFD calculations requires to include both the "work term" and the "convective term" in the modeling of the boundary layer.

However, all models above should not be applied to engine flows, which cannot be considered isothermal at all as near-wall gas temperatures are relevantly higher than wall temperatures during compression and combustion. This is the reason why several authors decided to propose wall heat transfer models able to account for variations of density (compressibility of the gas mixture) and even variations of all other gas properties (such as viscosity) with temperature. Among these "non-isothermal" models two of the most diffused are the Angelberger [26] and the Han and Reitz [27] ones. A deepening on these models can be found in Appendix, which may help to understand better the rationale of the alternative wall function proposed in the present paper. Both formulations aim to account density variation within the boundary layer. The first one includes the variation of viscosity with temperature, while the second one takes into account the increase of the turbulent Prandtl number in the buffer and viscous sublayer. From a practical point of view, the models are pretty similar as the expression of the wall heat flux is shared and the logarithmic law of the wall differs slightly in the constants, as visible in Table 3. Thus the Han and Reitz model provides higher heat fluxes (when y^+ falls within the inertial sublayer) if compared to the Angelberger one. The main difference between the two models is that Han and Reitz do not introduce a secondary (linear) law of the wall for the viscous sublayer. Moreover, in [27] they propose also a more complex version of the heat flux expression (not reported here), enabling to account for heat generation due to chemical reactions.

Other authors tried to propose models suited for non-isothermal flows (i.e. able to account for gas compressibility and sensitivity of properties to temperature). Nuutinen's work should be mentioned [16], in which the proposed model solves simplified boundary layer equations for enthalpy, momentum, turbulent kinetic energy and dissipation in wall adjacent cells. The boundary layer equations include temperature gradient-induced density and property variations and complete imbalance contributions (such as convection, transient terms, pressure gradients and external sources) which were completely neglected by Angelberger. However, if compared to Angelberger's, Nuutinen's results are similar even if the methods are pretty different, because Angelberger enhances the predicted heat fluxes amplifying the effect of strong density variations, while Nuutinen method is affected by imbalance effects. Reitz proposed another wall heat transfer model in [28], based on the one-dimensional unsteady energy equation solution aiming to account unsteadiness. Gas compressibility is also considered in the heat transfer model formulation by means of a Lagrangian coordinate transformation in the wall region. The same rationale is applied to the k-ε turbulence model to account for the effect of density variations on turbulent boundary conditions. Recently, Saric et al. [29] proposed a "hybrid" wall heat transfer model able to blend the exact boundary condition (used for the integration up to the wall) with the wall function (adopted with a high-Reynolds number approach), allowing well-imposed boundary conditions for any position of the near-wall computational node. The potential of this method to face complex flows is high, mostly from the industrial practice point of view, as the first grid node may lie either in the viscous or in the inertial layer or even between the two (buffer zone). Saric et al. derived the idea from Popovac and Hanjalić [30] and Kader [31] for the dimensionless temperature profile blending formula. It is also of paramount importance to point out that the turbulence model employed by Saric et al. is a k-ζ-f RANS model able to account for the wall-proximity effects when the first grid node lies in the viscous sub-layer or in the buffer zone. This is fundamental when such hybrid treatments of wall boundary conditions are used, as they require a turbulence model allowing the integration up to the wall. Finally, another wall heat transfer model was proposed by Rakopoulos et al. [15], whose efforts led to a formulation including the "work" term (pressure derivative over time) and the "combustion" term (volumetric heat release rate due to combustion chemical reactions), which, according to the authors, should not be neglected. They were able to demonstrate that, at least for the analyzed engines, the "unsteady" and the "convective" terms could be ignored since they compensate themselves mutually. Furthermore, following Han and Reitz's methodology [27], Rakopoulos et al. were also able to account for density variations within the boundary layer.

3.2 An Alternative Proposal

As it will be shown in the "Preliminary Results" paragraph, the most diffused wall heat transfer models accounting for boundary layer density variations (such as the Angelberger's or the Han and Reitz's ones) usually provide an overestimation of the global heat flux if compared to the target extrapolated by the experimental engine thermal survey. Therefore many existing models have been critically analyzed and an alternative formulation is proposed. In particular the wall heat transfer model presented in this paper (a similar version of which was already defined by Angelberger in [32] as "ad-hoc" remedy) differs from those presented above because of the different scales of velocity, temperature and wall distance introduced for the inner zone of the boundary layer

$$u_\tau^* = \sqrt{\frac{\tau_w}{\rho^*}} \qquad T_\tau^* = \frac{q_w}{\rho^* \cdot c_p . u_\tau^*} \qquad y_\tau^* = \frac{\nu^*}{u_\tau^*} \qquad (2)$$

where ρ^* and ν^* are the mean density and viscosity of the inner zone (values at the centroid of the near wall cell are used). These scales are used to obtain non-dimensional wall distance and temperature respectively:

$$y^{+*} = \frac{y}{y_\tau^*} \qquad T^{+*} = \frac{T_w - T}{T_\tau^*} \qquad (3)$$

Moreover, unlike Kays and Crawford (which assumed constant gas properties inside the inner zone of the boundary layer, equal to the wall ones) and Angelberger (which accounted for property variability in the same zone), the energy equation adopted in this approach assumes constant gas properties (e.g. c_p^*, λ^*, μ^*) equal to mean values of the inner zone, similarly to ρ^* and ν^*. Therefore, starting from such equation and using the dimensionless distance and temperature in (17) (assuming that all the previous assumptions such as negligible pressure gradient or quasi-steady flow are still valid), the new dimensionless equation simplifies as follows:

$$\left(\frac{1}{Pr^*} + \frac{\nu^{+*}}{Pr_t^*}\right)\frac{dT^{+*}}{dy^{+*}} = 1 \qquad (4)$$

where ν^{+*}, Pr^* and Pr_t^* are evaluated by means of mean quantities of the inner zone.

Similarly to the Angelberger's model, all the considerations made by Kays and Crawford are supposed still valid even if the flow is not isothermal; so the non-isothermal law of the wall has the same form as the isothermal one proposed by Kays and Crawford, the difference being the choice of the variables used to account for the variation of gas properties with temperature. In other words, an isothermal law of the wall can be applied to non-isothermal problems if variables are made dimensionless by means of mean thermodynamic properties (ρ^* and ν^*) of the inner zone rather than wall properties (ρ_w and ν_w). As a consequence:

$$T^{+*} = 2.075 \cdot ln(y^{+*}) + 13.2 \cdot Pr^* - 5.34 \qquad (5)$$

However, compared to the so-called "ad-hoc" heat transfer model, in the proposed approach Pr^* is not constant but it is allowed to vary. In other words, although Pr has to be considered a constant during a single time step because of the quasi-steady assumption, for the same hypothesis, time step by time step, Pr can vary to follow gas property changes. In fact, unlike Kays and Crawford's or even Angelberger's wall functions which assume constant Pr in space (i.e. in the internal zone of the BL along the direction normal to the wall) and time, Pr^* is here constant in space but not in time: it is recomputed every time step for each near wall cell according to specific heat, thermal conductivity and dynamic viscosity evaluated based on the local temperature. Moreover it should be noted that Pr^* number is kept constant in space in order to guarantee mathematical consistency during the integration of the simplified dimensionless energy equation. In Kays and Crawford's demonstration [24], law of the wall expression is obtained integrating energy equation as follows

$$T^+ = \int_0^{13.2} Pr\, dy^+ + \int_{13.2}^{y^+} \frac{Pr_t\, dy^+}{k y^+} \qquad (6)$$

and admitting that Pr number is a constant with respect to y^+. As specified above, the expression of the wall function in the proposed heat transfer model is the same as the Kays and Crawford's one despite the variable change (T^+ and y^+ become T^{+*} and y^{+*} respectively); this is the reason why Pr number (Pr^*) is kept constant in space. To further remark, the approach proposed in this paper accounts for mean gas properties in the inner zone. That is to say, these quantities such as density and viscosity are allowed to vary in the inner zone, coherently with a "non-isothermal" approach, but constant mean values along the direction normal to the wall are taken into account. Thus also Pr number (Pr^*) is a constant, being dependent on the gas properties.

Also for this alternative approach, the logarithmic expression of the dimensionless temperature (T^{+*}) is valid only for the inertial sublayer. As for the viscous sublayer, the simplified formulation $T^{+*} = Pr^* \cdot y^{+*}$ is adopted. The switching point is still y_{sw}^{+*} =13.2.

Finally the expression of the heat flux results in:

$$q_w = -\frac{\rho^* \cdot c_p^* \cdot {u_\tau}^* \cdot (T - T_w)}{T^{+*}} \qquad (7)$$

Kays and Crawford	$q_w = -\frac{\rho_w \cdot c_p \cdot u_\tau \cdot (T - T_w)}{T^+}$	$T^+ = 2.075 \cdot \ln(y^+) + 3.9$ $T^+ = Pr \cdot y^+$	$y^+ > 13.2$ $y^+ \leq 13.2$
Angelberger	$q_w = -\frac{\rho_w \cdot c_p \cdot u_\tau \cdot T_w \cdot ln\left(\frac{T}{T_w}\right)}{\theta^+}$	$\theta^+ = 2.075 \cdot \ln(\eta^+) + 3.9$	$\eta^+ > 13.2$ $\eta^+ \leq 13.2$
Han and Reitz	$q_w = -\frac{\rho_w \cdot c_p \cdot u_\tau \cdot T_w \cdot ln\left(\frac{T}{T_w}\right)}{\theta^+}$	$\theta^+ = 2.1 \cdot \ln(\eta^+) + 2.5$	$All\ \eta^+$
Alternative Model	$q_w = -\frac{\rho^* \cdot c_p^* \cdot {u_\tau}^* \cdot (T - T_w)}{T^{+*}}$	$T^{+*} = 2.075 \cdot ln(y^{+*}) + 13.2 \cdot Pr^* - 5.34$ $T^{+*} = Pr^* \cdot y^{+*}$	$y^{+*} > 13.2$ $y^{+*} \leq 13.2$

Table 3. Wall Heat Transfer Models

4. Integrated In-Cylinder / CHT Methodology and Numerical Setup

4.1 General Guidelines

The point-wise thermal field of an internal combustion engine is affected by several cross-linked factors such as the total amount of wall heat flux and its spatial distribution over the engine components, the heat removal effectiveness of the coolant circuit, the heat flux due to frictions and finally the cooling effect due to the lubricating circuit and the environment. In order to simulate well the engine temperature distribution, the authors developed an integrated in-cylinder / CHT method [33,34] whose scheme is reported in Figure 3, aiming to account for all the phenomena discussed above.

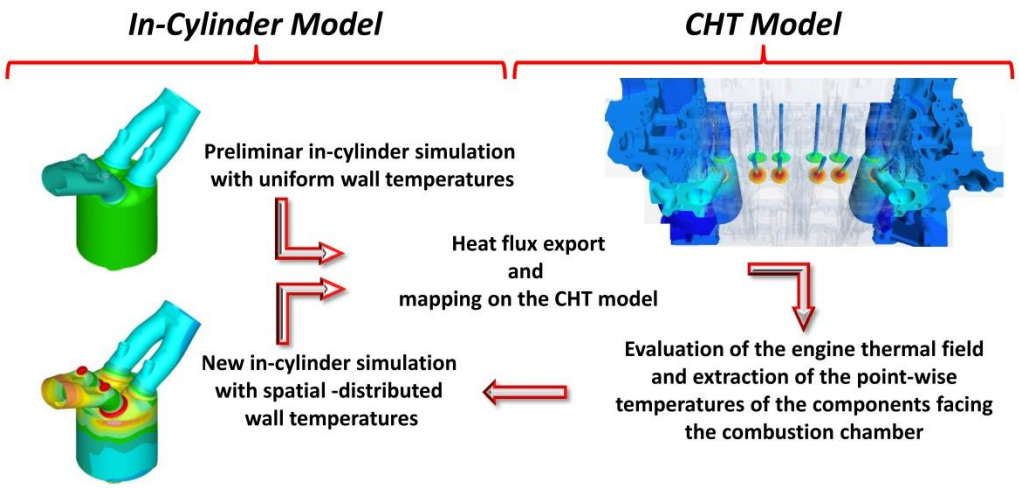

Figure 3. Integrated in-cylinder / CHT methodology scheme

A preliminary in-cylinder full-cycle simulation with uniform wall temperatures on the boundaries facing the combustion chamber is run to extract cycle averaged point-wise thermal loads. These are passed as a thermal boundary condition to the CHT model of the whole engine, in which solid components (such as head, block, gasket, valves, valve seats, valve guides and liners) are simulated together with the coolant circuit in order to evaluate simultaneously both the engine thermal field and the heat removed by the coolant. It is worthwhile to point out that the thermal inertia of the solid components facing the combustion chamber is high enough not to be sensible to cycle-resolved thermal loads. Relying on this assumption, the adoption of cycle-averaged heat fluxes is justified. Wall temperatures provided by the CHT simulation are then mapped back onto the boundaries of the in-cylinder model. The in-cylinder simulation is then repeated using the point-wise temperature distribution as a boundary condition, which is able to influence both globally and locally the heat transfer through the walls. Once again the resulting wall heat fluxes are cycle-averaged and used to update the engine thermal field in the CHT model. In order to achieve convergence in terms of engine thermal field between the two simulation realms, authors' experience suggests that the interaction (which takes place as data exchange) between the two frameworks has to be performed no more than twice.

4.2 In-cylinder Model

A customized version of STAR-CD v4.22 licensed by CD-adapco is used to carry out the in-cylinder 3D-CFD simulations presented in this paper. Time dependent pressure and temperature boundary conditions derived from calibrated 1-D models of the engines (supplied by engine manufacturers) are imposed. Simulations are run in a RANS framework and turbulence is modeled by means of the k-ε RNG model for compressible flows, with a high-Reynolds approach for the near-wall treatment. All the investigated engines (A, B, C, and D) are simulated by means of a

computational mesh covering the overall combustion system of one cylinder, including the in-head portions of the intake and exhaust ports; even if exploitable, geometrical symmetry was not exploited. Total number of fluid cells at TDC is about 700.000 for engines A and B and 500.000 and for engines C and D; layer addition and removal is adopted to account for mesh motion, leading to a maximum of 1.5 million cells for engines A and B and 1 million cells for engines C and D at BDC. A pre-atomized population of Lagrangian particles is assigned to each of the injector nozzles of the analyzed engines by means of user coded routines for the high-pressure fuel injection simulation, following the strategy described in [35]. The Reitz's model [36] is adopted for the modeling of the secondary break-up while the Bai's approach [37] is adopted for droplet wall interaction. ECFM-3Z [38] is used as combustion model, since it was widely used in previous publications by the authors [3, 4, 17, 19, 21]. The thermal loss caused by the presence of cooled walls is accounted for by means of the flame quenching model proposed by Bruneaux [39]. As the investigated engines are experimentally known as knock-safe, for the chosen engine operations no knock model is used, despite local knock effects on heat transfer were investigated by the authors in [17]. Two widely adopted heat transfer models available in the STAR-CD package and in many commercial codes are preliminarily evaluated. They are the Angelberger's [26] and Han and Reitz's [27] thermal wall functions respectively.

4.3 CHT Model

In order to account for the mutual interaction between the coolant circuit and the solid regions, CHT simulations are used. The temperature distribution of the engine components depends on both the cooling system effectiveness and the point-wise thermal load, so the three elements are strictly linked to each other. In other words, once the cooling system operating conditions are defined and the thermal load is imposed, the numerical thermal field has to match the experimental one. The computational domain includes the coolant circuit and all the surrounding solid components. Valves, seats and valve guides are added to capture well the heat transfer between the different elements. A contact resistance is set between adjacent regions to emulate temperature discontinuities. A typical CHT computational domain and its CFD grid are schematically represented in Figure 4.

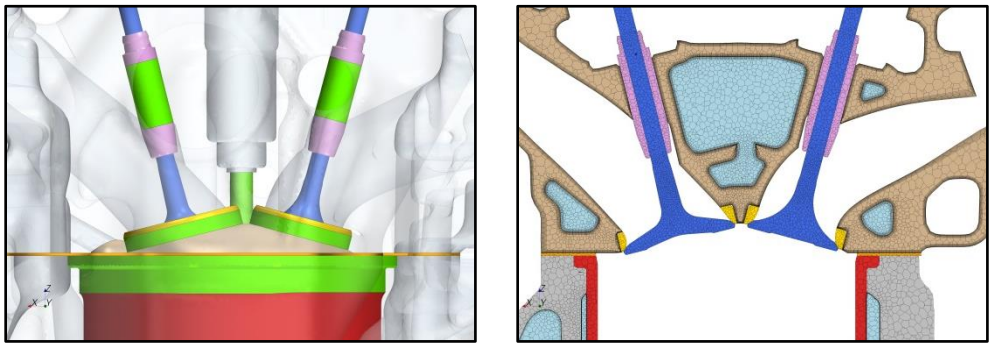

Figure 4. On the left some of the components (such as valves, valve seats, valve guides, liner) consituting the computational domain. On the right a section passing through the valve axes representing the CFD grid on both the fluid (light blue colour) and the solid side

As stated in the General Guidelines section, the thermal boundary conditions are time-invariant, i.e. the heat fluxes are not cycle-resolved because of the thermal inertia of the solid components. Similar considerations apply for the treatment of moving elements (such as valves), which are placed in a fixed position. The only exception is the piston: because of its continuous motion within the liner, it cannot be placed in fixed position, and it is not included in the computational domain. Nevertheless, the heat exchanged with the cylinder liner is accounted for by means of a dedicated CFD model, whose details are given in [33] . Despite the time independence of the thermal boundary conditions, a transient solver is needed due to the adoption of a multiphase boiling model which accounts for phase transition in the coolant circuit and the related local heat transfer increase. A combination of numerical and experimental data are used to obtain other boundary conditions such as the coolant mass flow rates and temperatures at the cooling circuit inlets/outlets, while the effects of the lubricating circuit and the external environment are represented by a pair of properly defined heat transfer coefficients and reference temperatures.

As for the cycle-average point-wise distributions of wall heat fluxes, they are directly applied on the combustion dome and the intake and exhaust ports. Thermal loads on the valve faces and stems are circumferentially averaged to take into account their rotation along the valve axes. The valves are placed in their closed positions and the lack of contact during a portion of the engine cycle is accounted for by means of a proper contact resistance.

As stated above, the piston is separately analyzed. Heat flux due to friction and conductive heat transfer from the piston skirt are used to increase the point-wise heat flux on the liners. It should be pointed out that each contribution is again cycle averaged and it is applied only on the cylinder liner portion affected by it. In particular, frictions due to rings and skirt are evaluated by means of the instantaneous in-cylinder pressure trace and split between liner and piston. As for the heat flux due to conduction between the piston skirt and the liner, it is evaluated through dedicated piston simulations in which the effects of oil jets, frictions, piston rings, coolant circuit and combustion heat fluxes are simultaneously taken into account. Further details on the methodology can be found in [21].

5. Preliminary Results

5.1 GM Pancake Engine

As specified for the in-cylinder model setup, two wall heat transfer models available in STAR-CD (Angelberger's and Han and Reitz's ones) were at first adopted for the simulations of the investigated engines. However, since several wall functions were validated by means of the GM pancake

engine, among which also the two tested ones, first of all the test case was reproduced in the STAR-CD framework to verify the possibility of replicating the encouraging results provided in the reference original papers of the models.

The GM pancake test case is a SI engine, fueled with premix air-propane mixture. The spark is central mounted and some geometrical characteristics are reported in Table 4. Point-wise wall heat flux measurements are available thanks to the experimental tests described in [9, 10]. Lack of information about the open-valve portion of the cycle forces to start the simulation at 117°CA bFTDC (which corresponds to IVC) and end at 80°CA aFTDC. So, as in previous studies available in literature, the gas exchange is not modeled. The simulation domain consists of an axisymmetric pancake geometry. Initial and boundary conditions are widely discussed in [29, 32] and briefly reported in Table 4 with some information about the investigated operating condition.

Geometrical Features	Bore	105 [mm]
	Stroke	95.25 [mm]
	Connecting Rod Length	158 [mm]
	Compression Ratio	8.56
Operating Condition	Engine Speed	1500 [rpm]
	Equivalence Ratio	0.87
	Volumetric Efficiency	40 %
	Spark Timing	27° CA bFTDC
Initial Conditions	TKE (k)	84 [m^2/s^2]
	Length scale (L)	0.93 [cm]
	Pressure	0.821 [bar]
	Temperature	449 [K]
	Axial Velocity w [z-direction]	Decreasing linearly from the piston velocity (at the surface of the latter) to 0 (at the cylinder head)
	Swirl Ratio (Radial Velocity u,v [x,y-directions])	1
	Mass Composition	Y_{C3H8}= 4.6 % Y_{O2}= 18.76 % Y_{N2}= 73.70 % Y_{CO2}= 1.89 % Y_{H2O}= 1.04 %
Boundary Conditions	Wall Temperatures	T_{Head}= 445 K T_{Liner}= 405 K T_{Piston}= 445 K

Table 4. Pancake engine geometrical data, investigated operating condition and initial and boundary conditions

The adopted computational grid contains approx. 700.000 cells at 117°CA bFTDC and about 300.000 cells at TDC, with a uniform near wall layer size of 1 mm. Thanks to the available experimental pressure trace, the combustion model (ECFM-3Z) as well as the ignition one are tuned. The comparison between numerical CFD and experimental data is reported in Figure 5.

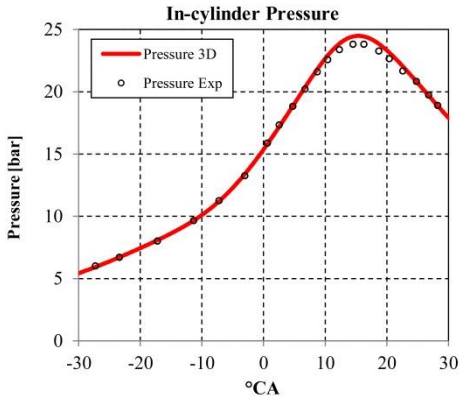

Figure 5. Experimental in-cylinder pressure trace for the Pancake engine and CFD calibration

After simulation tuning, numerical and experimental data are compared in terms of wall heat flux. As stated before, point-wise wall heat flux measurements are available thanks to experimental tests. In particular four probes are available on the cylinder head (here referred to as HT1 to HT4) and one on the liner (referred to as HT5). The radial distances of probes HT1, HT2, HT3 and HT4 from the central mounted spark plug are 18.7, 27.5, 37.3 and 46.3 mm, respectively. On the liner, HT5 is located 6.3 mm below the head. Because of its importance for the simulation of both the flow and the thermal fields, y+ is monitored at all probe locations. For sake of brevity, wall heat flux and y^+ are reported only for the HT1 probe in Figure 6.

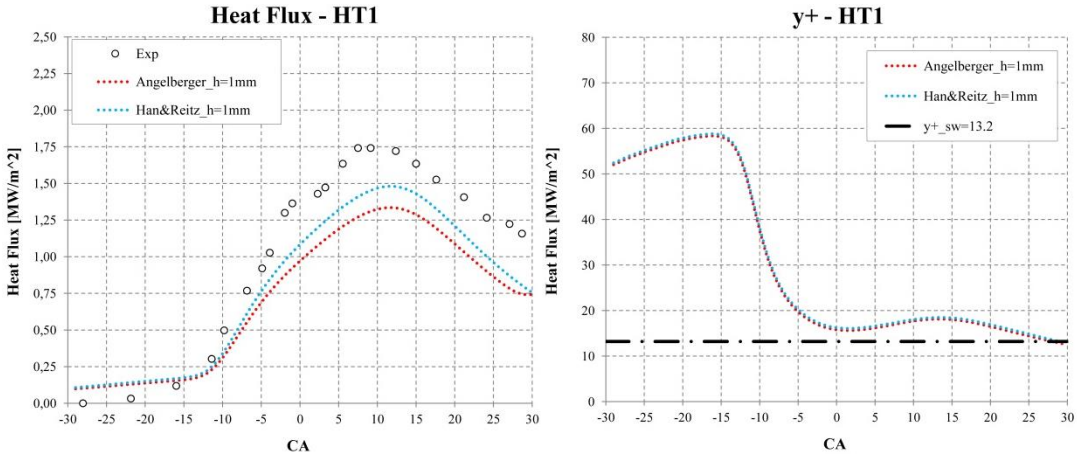

Figure 6. On the left wall heat fluxes on the probe HT1 provided by experiments and numerical simulations. On the right wall y^+ (evaluated following Angelberger / Han and Reitz methodology so it is, in practice, η^+)

As visible, numerical heat fluxes appear close to the experimental evidences.

5.2 Current Production Engines

Starting from the encouraging results obtained with the GM pancake test case engine, both heat transfer models are applied to current production SI, direct injected, turbocharged, high specific power engines. In-cylinder simulations are performed on the four investigated engines (previously described and called A, B, C and D) to obtain gas-to-wall heat fluxes, whose application in CHT analyses is described above. 3D CFD simulations are preliminarily tuned to match the in-cylinder average pressure trace. As for ignition, a relatively simple flame kernel deposition model is used , which is released close to the experimental spark timing (to account for the arc delay); injected fuel, trapped mass, start of injection angle (SOI) and valve lift perfectly match the actual engine operations. Several subsequent engine cycles are run for each operating condition to achieve a fully converged solution. In Figure 7 dimensionless numerical 3D-CFD curves of in-cylinder pressure are compared with the experimental or 1D traces (which are calibrated, in turn, on the experimental ones), based on the available data.

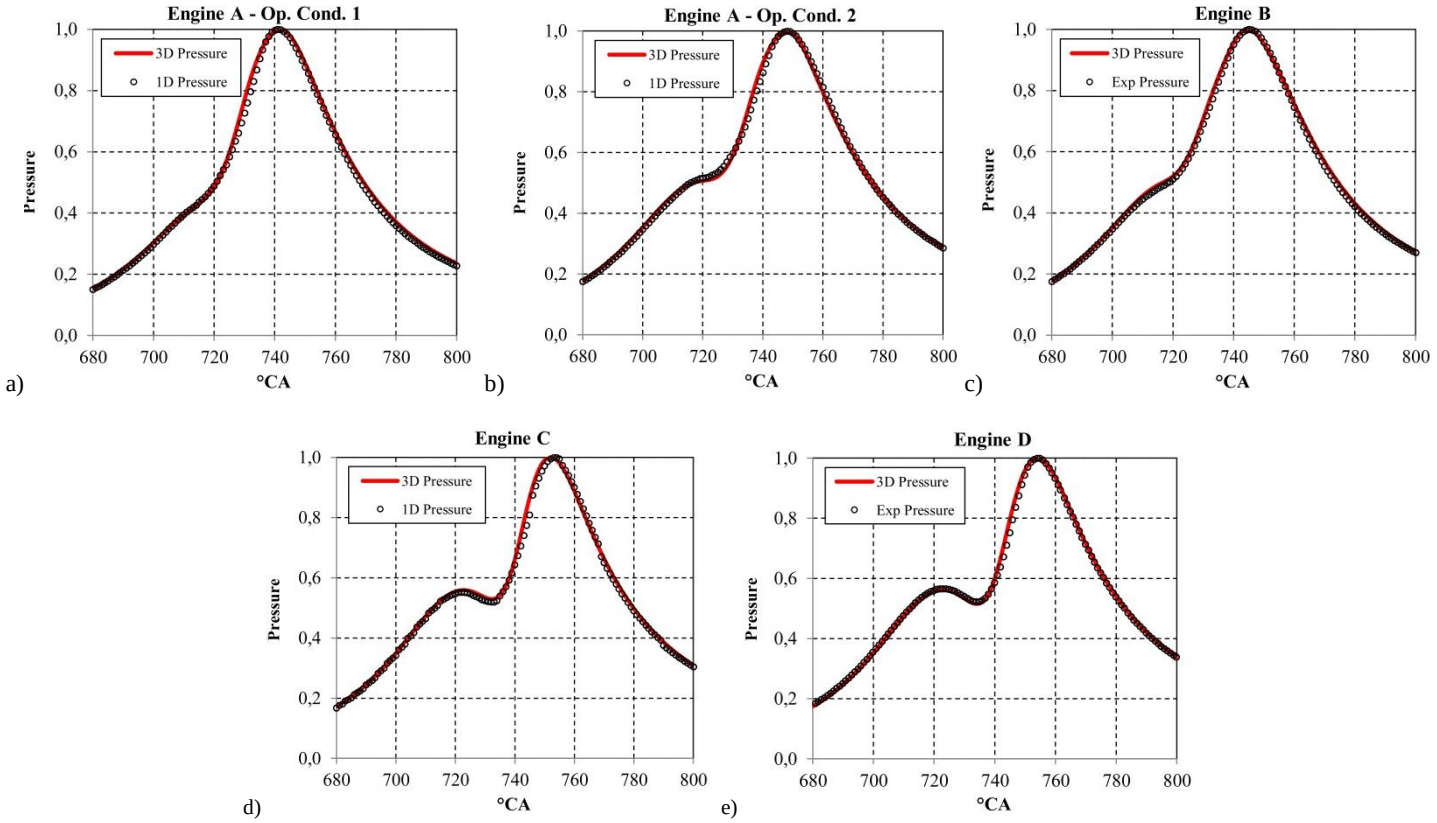

Figure 7. Comparison between 1D-CFD or Experimental and 3D-CFD in-cylinder pressure traces for Engine A Operating condition 1(a), Engine A Operating condition 2 (b), Engine B (c), Engine C (d), Engine D (e)

After combustion tuning, the analysis focuses on the heat transfer estimated by means of the two selected models (the Angelberger's and the Han and Reitz's ones). As stated in the introduction, experimental heat flux measurements are far beyond the usual industrial practice and public data provided in literature deal with operating conditions far from the high-speed full-load analyzed ones. Nonetheless, available experimental engine heat rejection thermal balances are able to provide the global time-averaged heat flux that should be released during combustion to the chamber and port walls. Assuming a similar combustion process (so a similar thermal loss) among all the cylinders, time-averaged heat flux targets are found for the in-cylinder 3D CFD simulations.

Figure 8 shows the numerical 3D CFD instantaneous boundary heat transfer calculated by means of the Angelberger's wall functions for operating condition 1 of Engine A. In particular, the red dashed line represents the numerical instantaneous total amount, for a single cylinder, given by the sum of the contributions on each combustion chamber component. Cycle-averaging this quantity, the solid red line is obtained. However, just a portion of this thermal load is used in the CHT model. In fact, as discussed above in the CHT model description, piston is not included in the computational domain and its estimated contribution to the cylinder liner is not the entire wall heat flux flowing through the piston crown, but just a portion of it. Once such portion is estimated (through a dedicated piston modelling framework), it is summed to the wall heat fluxes acting on all the other boundaries (cylinder liner, dome, valves and ports) to give the amount represented by the dotted solid red line in Figure 8. Such quantity can be finally compared to the target average heat transfer extrapolated from the experimental engine thermal survey (previously discussed) which is represented by the solid black line with crosses. The graph represented in Figure 9 is analogous to the previous one, but this time the reported quantities are calculated by means of the Han and Reitz's heat transfer model (in light blue colour).

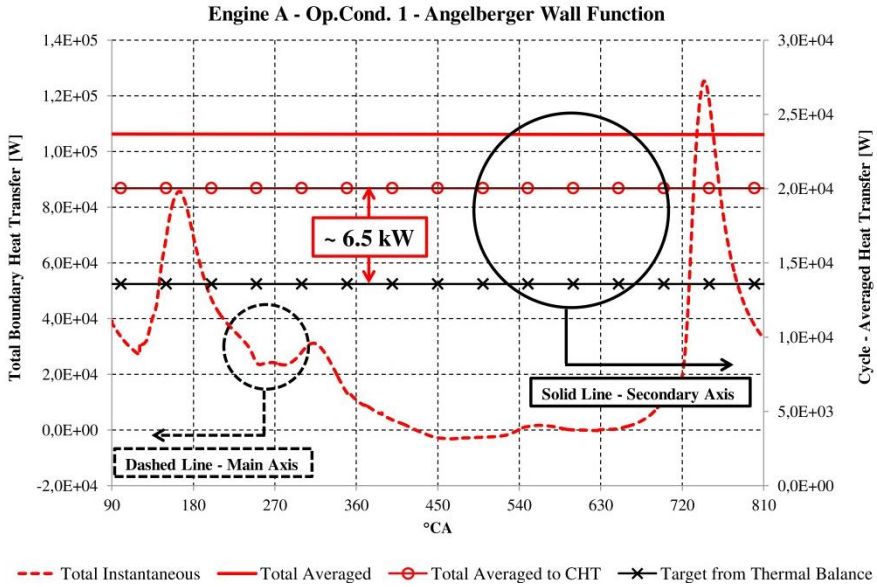

Figure 8. Total boundary heat transfer (instantaneous and cycle-averaged) for a single cylinder of the Engine A Op.Cond.1; the numerical one is obtained by means of the Angelberger heat transfer model

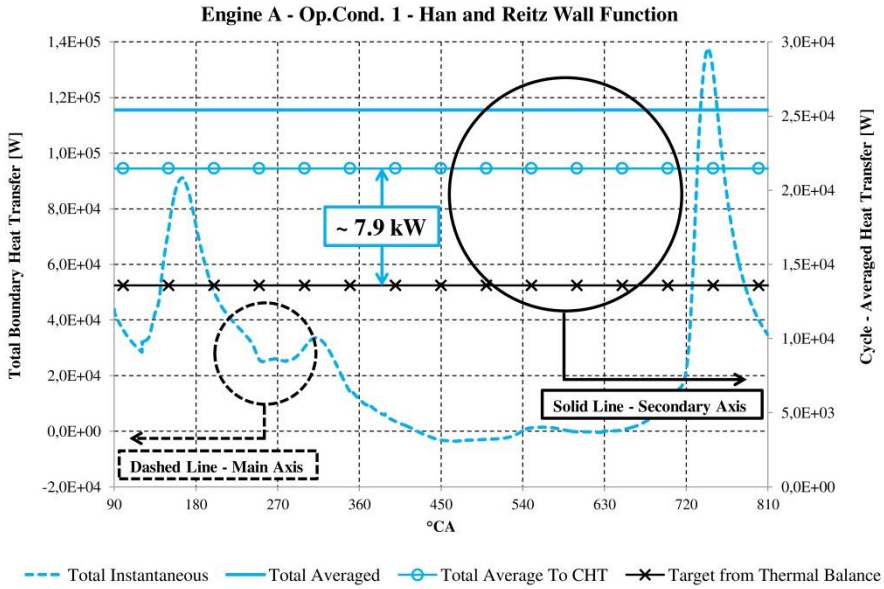

Figure 9. Total boundary heat transfer (instantaneous and cycle-averaged) for a single cylinder of the Engine A Op.Cond.1; the numerical one is obtained by means of the Han and Reitz heat transfer model

The results concerning all the engines and the operating conditions are briefly resumed in the following histogram for sake of brevity, as they show very similar trends. In particular, the cylinder cycle-averaged wall heat transfer is reported for each engine and for both the selected heat transfer models. Results are reported in a dimensionless form to highlight the discrepancy between predicted and target data.

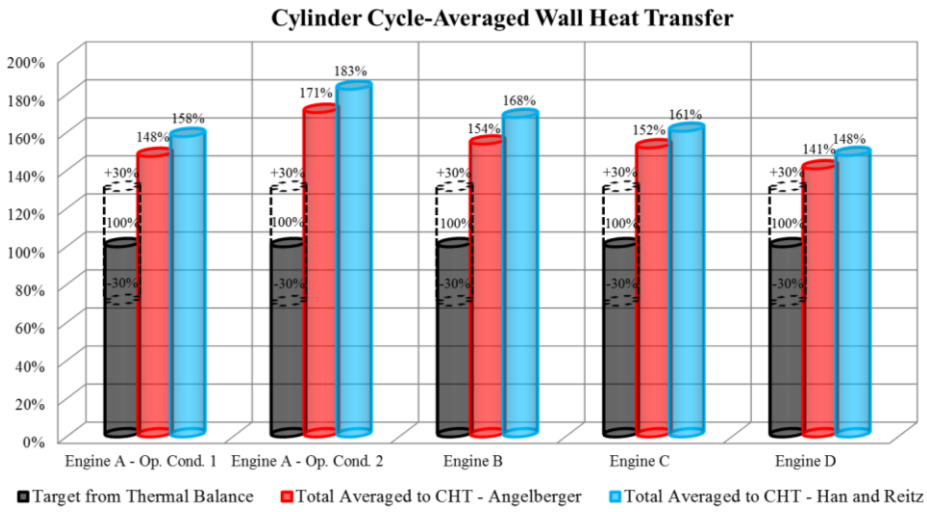

Figure 10. Cycle-averaged total boundary heat transfer for engines A (Op.Cond.1 and 2), B, C and D

Figure 10 shows a relevant overestimation of the heat fluxes through the combustion chamber walls provided by both heat transfer models. In particular, time-averaged values predicted by the numerical analyses exceed by even more than 50% the value inferred from the engine experimental thermal survey. Since the selected laws of the wall differ for just the value of the constant term, which is higher in Angelberger's formulation, the heat transfer predicted by the Han and Reitz's model is slightly higher as depicted by the histogram in Figure 10.

Such overestimation is also confirmed by the numerical-experimental comparison in terms of engine temperature distribution: engine thermal fields predicted by the CHT models are unacceptably higher than the experimental ones. Comparing simulation results for the investigated engines with the experimental temperatures (not available for engine B) measured by means of several thermocouples placed in the most interesting engine locations, it is clearly visible that the simulated engine thermal field is always overestimated for both the engine head and block. This is a consequence of the overprediction of the heat fluxes calculated by means of the selected heat transfer models. For the sakes of brevity Figure 11 shows such comparison only for Engine A operated at condition 1.

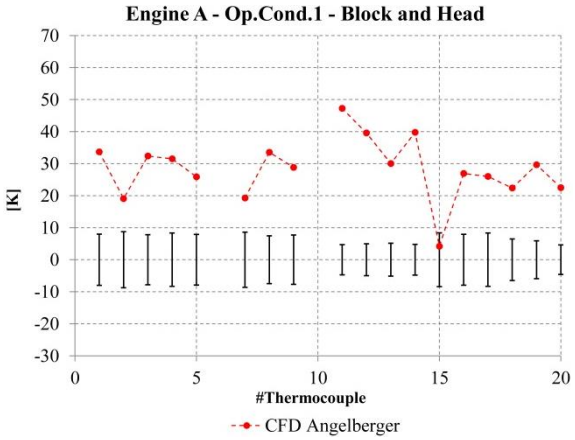

Figure 11. ΔT ($=T_{CFD}-T_{EXP}$) between numerical and experimental temperatures is reported for Engine A @ Op.Cond. 1

Finally, the inconsistency of the heat transfer is confirmed by the comparison between the numerical temperature of the coolant exiting the engine and the experimental one.

6. Application of the proposed model

The proposed alternative wall heat transfer model is then applied to the investigated current production engines. The computed wall heat fluxes result much lower than those provided by both Angelberger's and Han and Reitz's models and much closer to the target value from the experimental engine thermal survey, as visible in Figure 12.

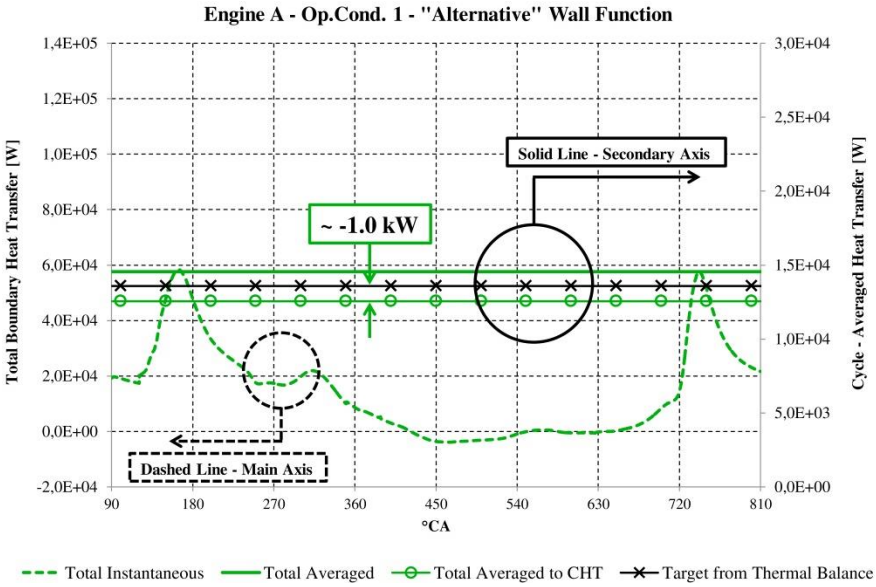

Figure 12. Total boundary heat transfer (instantaneous and cycle-averaged) for engine A Op.Cond.1, provided by the "alternative" wall function

Figure 13 reports the results concerning all the engines and the operating conditions.

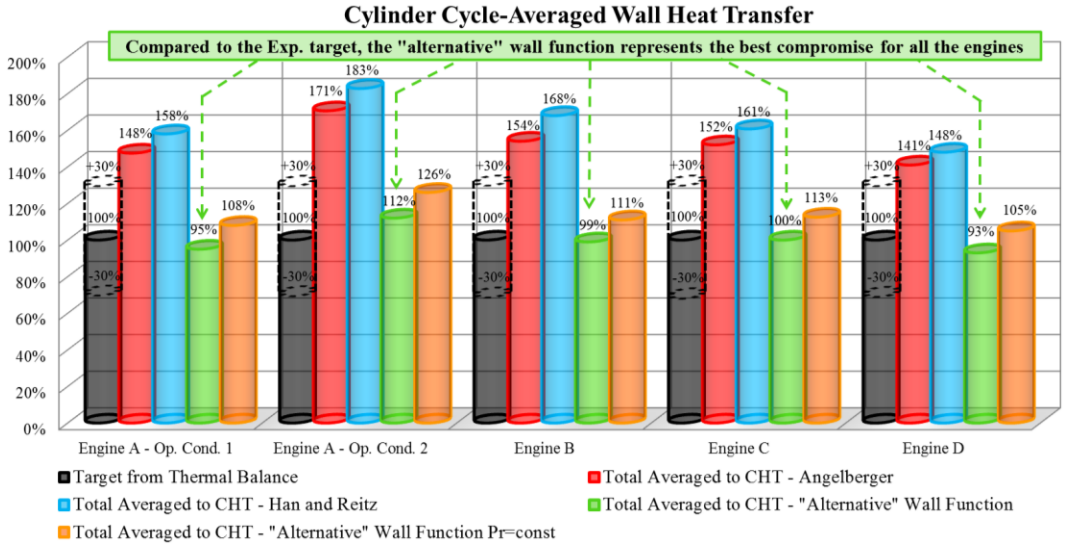

Figure 13. Cycle-averaged total boundary heat transfer for engines A (Op.Cond.1 and 2), B, C and D

For all the analyzed engines and conditions, a very good agreement is achieved between numerical and experimental data thanks to the proposed heat transfer model. Moreover, the histogram in Figure 13 allows to appreciate the importance of having a variable Pr number which, as previously discussed, characterizes the proposed law of the wall if compared with the most diffused heat transfer models. In order to point out the essentiality of such peculiarity, the orange columns of the histogram above report results (for all the operating conditions) obtained imposing a constant Pr number equal to 0.7. In other words, nothing changes with respect to the proposed alternative heat transfer model apart from the adopted law of the wall (5), which assumes an easier form as in equation (18) or even (22) reported in Appendix, in which Pr number is a constant; dimensionless variables and heat flux formulation remain those of the proposed alternative approach (i.e. as in (3) and (7)). As visible, a constant Pr number implies higher wall heat fluxes, relevantly farther from the experimental target.

Starting from such very encouraging results, heat fluxes provided by the proposed alternative heat transfer model are used as thermal boundary conditions in a new set of CHT simulations whose outcomes in terms of engine temperature field are reported below and compared with experimental data.

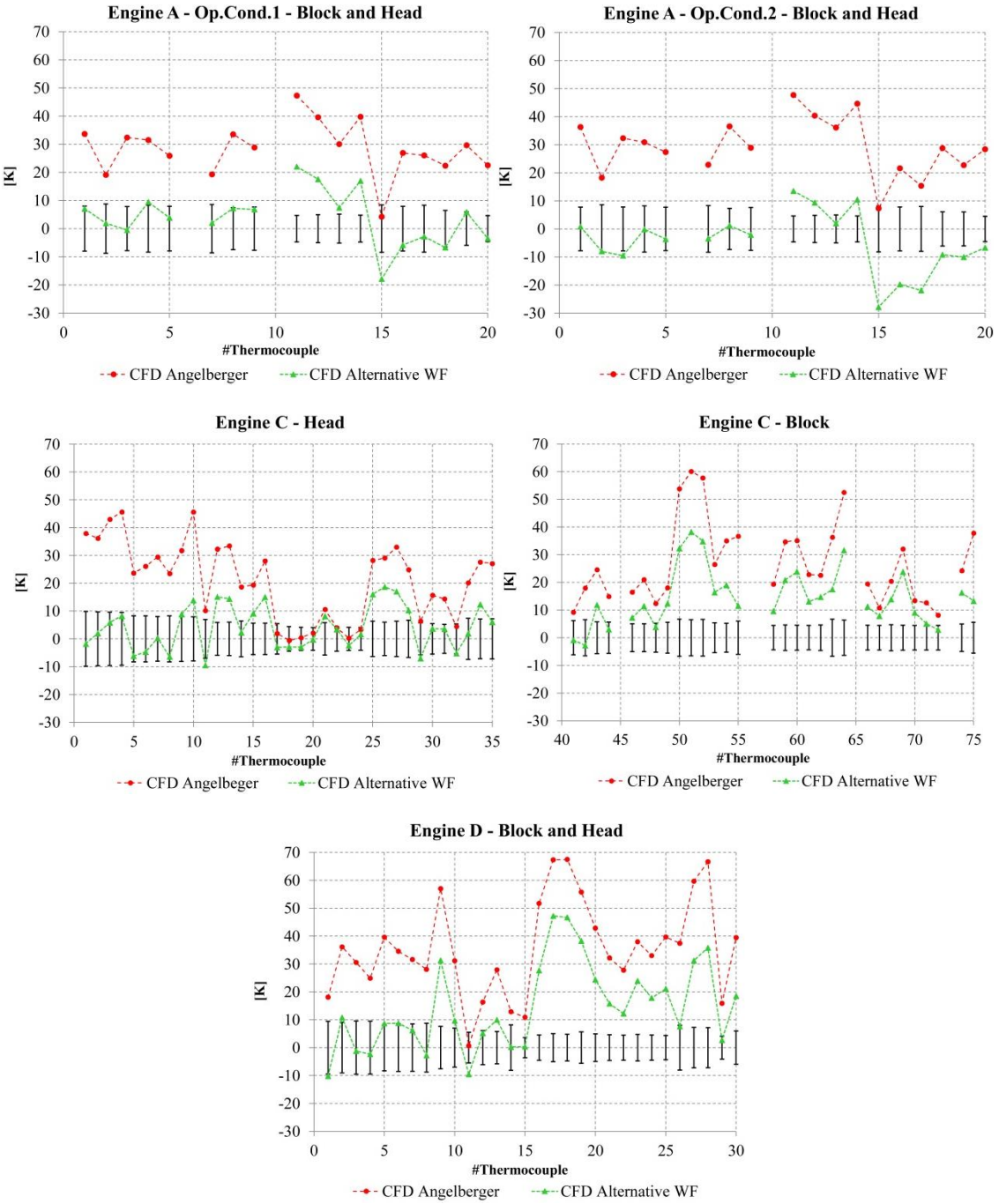

Figure 14. ΔT (=T_{CFD}-T_{EXP}) between numerical and experimental temperatures is reported for engine A (@ Op.Cond. 1 and 2), engine C and D

Thanks to the accuracy of the numerical wall heat transfer, which satisfies perfectly the experimental thermal balance of the engine, now the simulated thermal field is able to match well the experimental one, as visible in Figure 14. The latter exhibits also the uncertainties in the experimental values due to thermocouple tolerance (±0.4% of the measured temperature) and repeatability of the measures (repeatability error is always lower than 4%).

Before concluding, it is useful to clarify the reason why traditional and diffused heat transfer models match correctly the measurements under the test case conditions and fail for the investigated current production high specific power DISI turbocharged engines (where, instead, the alternative model works well). In order to explain such behavior the so-called "isothermicity parameter" ζ can be introduced. Such parameter represents, as visible in equation (8), both a characteristic scale of the ratio of the gas temperature to the wall temperature and a characteristic scale of the heat flux (it can be considered as a dimensionless heat flux). In fact it is:

$$\zeta = \frac{-T_\tau}{T_W} = \frac{-q_w}{\rho_w \cdot c_p \cdot u_\tau \cdot T_w} \qquad (8)$$

If ζ approaches zero, the heat flux becomes negligible as well as the difference between gas and wall temperatures. As a consequence, the boundary layer can be assumed quasi-isothermal and both viscosity and density are nearly constant. Therefore "classical" and older heat transfer models (such as the Kays and Crawford's or the Launder and Spalding's ones) can be adopted. Otherwise, if ζ is not negligible, even the heat flux is not and the gas properties (temperature, density and viscosity) cannot be considered constant (and equal to the wall ones) within the boundary layer which, in turn, is not isothermal anymore. In this case, purposely dedicated models such as the Angelberger's and the Han and Reitz's ones have to be applied.

The evolution of the ζ parameter on the walls facing the combustion chamber is shown in Figure 15 for both the GM pancake and the investigated engines. For sakes of comparison ζ values are computed using the same heat transfer model (Angelberger) for all the engines and the operating conditions. The graphs show relevantly higher ζ values for the GM pancake engine compared to the current production high specific power ones. This is a consequence of in-cylinder turbulent kinetic energy and pressure. In fact, ζ can be rewritten, following the assumption of ideal gas, as follows:

$$\zeta = \frac{-q_w}{p \cdot u_\tau \cdot \gamma/(\gamma - 1)} \qquad (9)$$

where p is the in-cylinder pressure and $\gamma = c_p/c_v$. Despite the investigated current production engines are characterized by higher heat fluxes (q_w) because of the higher specific power, assuming an equal γ for all the engines, ζ is lower because of the much higher in-cylinder pressure (p) and friction velocity (u_τ). It should be pointed out that pressure and friction velocity are higher for current production engines because of their higher specific power (obtained by means of engine boosting) and turbulent kinetic energy, respectively. In fact, under the assumption of equilibrium in the inertial sublayer, friction velocity is evaluated by means of the turbulent kinetic energy, which is higher thanks to the high peak revving speeds and high tumble ratios.

Such behavior of the ζ parameter can be easily explained considering the heat transfer (q_w) as a product of a "heat transfer coefficient" and a "temperature difference". Compared to the pancake engine, the analyzed current production ones operated at high load and high revving speed are characterized by increased heat flux (q_w), which is due to a higher heat transfer coefficient rather than a higher temperature difference which is lower. In fact, introducing the Angelberger heat flux expression (14) in (22), ζ simplifies as follows:

$$\zeta_{Angelberger} = \frac{ln\left(\frac{T}{T_w}\right)}{\theta^+} \qquad (10)$$

which represents the "temperature difference" mentioned above and which is lower for current production engines as shown in Figure 15. In other words the heat flux for such engines is higher because of the higher in-cylinder pressure and turbulent kinetic energy (which affect the "heat transfer coefficient"), not for a hotter boundary layer thermal field which is colder at a same dimensionless distance, if compared to the pancake engine.

Concluding, such differences in terms of boundary layer temperature can motivate the use of different heat transfer models, based on the application. In fact Angelberger or even Han and Reitz heat transfer models, which emphasize the variation of density inside the boundary layer due to a high temperature gradient, prove to be valid for the prediction of wall heat fluxes at high ζ values (i.e. high temperature gradient), as in the pancake case. On the contrary, where the temperature gradient is less considerable, that is the boundary layer is more "isothermal" (as for the analyzed current production engines), the alternative heat transfer model proposed in the present paper shows better consistency with the available experimental data.

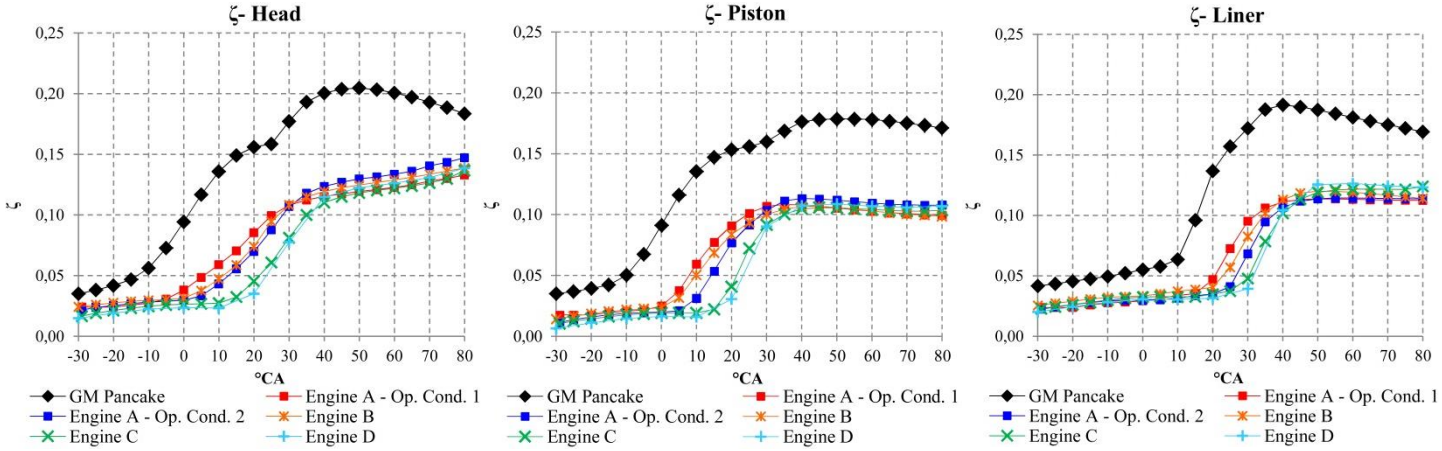

Figure 15: ζ on head, liner and piston of both the GM pancake engine and the investigated engines

7. Conclusions

Current production SI engines are characterized by high specific power achieved by means of different techniques such as turbocharging and downsizing. However, since the raise of the thermal loads can significantly reduce the mechanical resistance of the engine components, the increase of specific power is limited by the risk of thermo-mechanical failures. In order to prevent such damages, CFD-CHT and FE tools may be used to calculate the thermal field and thermo-mechanical stresses of the engine, reducing proficiently time- and cost-to market. For this purpose it is

fundamental to estimate correctly the gas-to-wall heat transfer, which affects not only the thermal stresses, but also the overall engine efficiency and the exhaust emissions.

Reliable wall heat fluxes acting on the components facing the combustion chamber are fundamental to calculate properly the thermal field of an ICE. Among the several models aiming to predict such heat fluxes, the paper tests the Angelberger's and the Han and Reitz's ones, being both widely available in CFD commercial codes. Even if both models prove to behave correctly when applied to a well-known engine test case (i.e. the GM pancake), they manifest evident shortages when used for highly-charged / highly-downsized, spark ignition engines. In particular, overestimations of the wall heat fluxes calculated by such thermal laws of the wall are pointed out thanks to experimental engine thermal surveys and temperature measurements on four current production engines.

In order to overcome such deficiencies a different heat transfer model is proposed in the present paper, which provides wall heat fluxes able to match both the experimental engine thermal survey and local temperature measurements for all the investigated engines and operating conditions. Moreover the adoption of the proposed heat transfer model for the 3D-CFD in-cylinder simulation of current production high performance DISI turbocharged engines operated at full load and high revving speed is motivated by the "isothermicity parameter" ζ. Such parameter points out the different boundary layer thermal state characterizing, on one hand, the GM pancake engine test case and, on the other hand, current production engines. Hence Angelberger or even Han and Reitz heat transfer models are still valid for the prediction of wall heat fluxes at high ζ values (i.e. high near-wall temperature gradients), as in the pancake engine case. On the contrary where the temperature gradient is less considerable, as for the analyzed current production engines, the alternative heat transfer model proposed in the present paper shows better consistency with the available experimental data.

References

1. Turner, J.W.G., Pearson, R.J., and Kenchington, S.A. "Concepts for improved fuel economy from gasoline engines," International Journal of Engine Research; January 1, 2005, vol. 6, 2, pp. 137-157. 4.
2. Fraser, N., Blaxill, H., Lumsden, G., and Bassett, M., "Challenges for Increased Efficiency through Gasoline Engine Downsizing," SAE Int. J. Engines 2(1):991-1008, 2009, doi:10.4271/2009-01-1053.
3. d'Adamo, A., Berni, F., Breda, S., Lugli, M. et al., "A Numerical Investigation on the Potentials of Water Injection as a Fuel Efficiency Enhancer in Highly Downsized GDI Engines," SAE Technical Paper 2015-01-0393, 2015, doi:10.4271/2015-01-0393.
4. Berni, F., Breda, S., D'Adamo, A., Fontanesi, S. et al., "Numerical Investigation on the Effects of Water/Methanol Injection as Knock Suppressor to Increase the Fuel Efficiency of a Highly Downsized GDI Engine," SAE Technical Paper 2015-24-2499, 2015, doi:10.4271/2015-24-2499.
5. Fontanesi, S., D'Adamo, A., Rutland, C.J., Large-Eddy simulation analysis of spark configuration effect on cycle-to-cycle variability of combustion and knock (2015) International Journal of Engine Research, 16 (3), pp. 403-418.
6. Fontanesi, S., and Giacopini, M., "Multiphase CFD-CHT optimization of the cooling jacket and FEM analysis of the engine head of a V6 diesel engine," Applied Thermal Engineering; Volume 52, Issue 2, 15 April 2013, Pages 293-303, ISSN 1359-4311, 10.1016/j.applthermaleng. 2012.12.005.
7. D J Oude Nijeweme, J. B. W. Kok, C. R. Stone, and L Wyszynski, "Unsteady in-cylinder heat transfer in a spark ignition engine: experiments and modeling", Proceedings of the Institution of Mechanical Engineers, Part D: Journal of Automobile Engineering June 1,2001 215:747-760, doi: 10.1243/0954407011528329
8. Myers, J. and Alkidas, A., "Effects of Combustion-Chamber Surface Temperature on the Exhaust Emissions of a Single-Cylinder Spark-Ignition Engine," SAE Technical Paper 780642, 1978, doi:10.4271/780642.
9. Alkidas, A.C. "Heat Transfer Characteristics of a Spark-Ignition Engine," ASME. J. Heat Transfer. 1980;102(2):189-193. Doi:10.1115/1.3244258.
10. Alkidas, A.C., Myers, J.P. "Transient Heat-Flux Measurements in the Combustion Chamber of a Spark-Ignition Engine," ASME. J. Heat Transfer. 1982;104(1):62-67. Doi:10.1115/1.3245069.
11. De Cuyper, T., Bracke, S., Lavens, J., Broekaert, S. et al., "Demonstrating the Use of Thin Film Gauges for Heat Flux Measurements in ICEs: Measurements on an Inlet Valve in Motored Operation," SAE Technical Paper 2016-01-0641, 2016, doi:10.4271/2016-01-0641.
12. B Lawton, "Effect of Compression and Expansion on Instantaneous Heat Transfer in Reciprocating Internal Combustion Engines", Proceedings of the Institutions of Mechanical Engineers, Part A: Journal of Power and Energy August 1978 201: 175-186, doi: 10.1243/PIME_PROC_1987_201_022_02.
13. Thermodynamics and Fluid Mechanics Group and W.J.D.Annand, "Heat Transfer in the Cylinders od Reciprocating Internal Combustion Engines", Proceedings of the Institution of Mechanical Engineers June 1963 177: 973-996, doi: 10.1243/PIME_PROC_1963_177_069_02.
14. Woschni, G., "A Universally Applicable Equation for the Instantaneous Heat Transfer Coefficient in the Internal Combustion Engine," SAE Technical Paper 670931, 1967, doi:10.4271/670931.
15. Rakopoulos, C. D., Kosmadakis, G. M., Pariotis, E. G. "Critical evaluation of current heat transfer models used in CFD in-cylinder engine simulations and establishment of a comprehensive wall-function formulation,", Applied Energy, 87, 2010, 1612-1630.
16. Mika A Nuutinen, Ossi T Kaario, Ville A Vuorinen, Paul N Nwosu, Martti J Larmi, " Imbalance wall functions with density and material property variation effects applied to engine heat transfer computational fluid dynamics simulations", International Journal of Engine Research April 2014 15: 307-324, first published on September 2, 2013 doi: 10.1177/1468087413481779.
17. Fontanesi, S., Cicalese, G., Cantore, G., d'Adamo, A. "Integrated In-Cylinder/CHT Analysis for the Prediction of Abnormal Combustion Occurrence in Gasoline Engines," SAE Technical Papers 2014-01-1151, DOI:10.4271/2014-01-1151.
18. Fontanesi, S., Giacopini, M., Cicalese, G., Sissa, S., Fantoni, S. "Numerical investigation of the cavitation damage in the wet cylinder liner of a high performance motorbike engine," Engineering Failure Analysis, Volume 44, September 2014, Pages 408–423, ISSN 1350-6307, http://dx.doi.org/10.1016/j.engfailanal.2014.05.025.
19. Fontanesi, S., Cicalese, G., d'Adamo, A., Cantore, G. "A Methodology to Improve Knock Tendency Prediction in High Performance Engines," ENERGY PROCEDIA, volume n. 45, pp. 769-778, ISSN: 1876-6102.

20. Fontanesi, S., Cicalese, G., and Giacopini, M., "Multiphase CFD-CHT Analysis and Optimization of the Cooling Jacket in a V6 Diesel Engine," SAE Technical Paper 2010-01-2096, 2010, doi:10.4271/2010-01-2096.
21. Cicalese, G., Berni, F., and Fontanesi, S., "Integrated In-Cylinder / CHT Methodology for the Simulation of the Engine Thermal Field: An Application to High Performance Turbocharged DISI Engines," *SAE Int. J. Engines*9(1):601-617, 2016, doi:10.4271/2016-01-0578.
22. Launder, B. E. and Spalding, D. B., (1974), "The numerical computation of turbulent flows", Computer Methods in Applied Mechanics and Engineering, 3(2): 269-289.
23. Jayatilleke, C. L. V. 'The influence of Prandtl number and surface roughness on the resistance of the laminar sublayer to momentum and heat transfer', in 'Progress in heat and mas transfer', Vol. 1, Pergamon Press, 1969.
24. W.M.Kays and M.E.Crawford, "Convective Heat and Mass Transfer. McGraw-Hill, New York, 3rd edition, 1994.
25. Huh, K., Chang, I., and Martin, J., "A Comparison of Boundary Layer Treatments for Heat Transfer in IC Engines," SAE Technical Paper 900252, 1990, doi:10.4271/900252.
26. Angelberger, C., Poinsot, T., and Delhay, B., "Improving Near-Wall Combustion and Wall Heat Transfer Modeling in SI Engine Computations," SAE Technical Paper 972881, 1997, doi:10.4271/972881.
27. Han, Z.; Reitz, R.D., "A Temperature Wall Function Formulation for Variable Density Turbulent Flows with Application to Engine Convective Heat Transfer Modeling," International Journal of Heat and Mass Transfer, Vol. 40, No. 3, pp. 613-625, 1997.
28. Reitz, R., "Assessment of Wall Heat Transfer Models for Premixed-Charge Engine Combustion Computations," SAE Technical Paper 910267, 1991, doi:10.4271/910267.
29. Saric, S. and Basara, B., "A Hybrid Wall Heat Transfer Model for IC Engine Simulations," SAE Int. J. Engines 8(2):411-418, 2015, doi:10.4271/2015-01-0388.
30. Popovac, M. and Hanjalic, K.: "Compound Wall Treatment for RANS Computation of Complex Turbulent Flows and Heat Transfer", Flow, Turbulence and Combustion, Vol.78, pp. 177-202, 2007, doi:10.1007/s10494-006-9067-x.
31. Kader, B.A.: "Temperature and Concentration Profiles in Fully Turbulent Boundary Layers," Int. J. Heat and Mass Transfer, Vol. 24, pp. 1541-1544, 1981, doi:10.1016/0017-9310(81)90220-9.
32. Angelberger, C. "Contributions à la modélisation de l'interaction 17lame-paroi et des flux pariétaux dans les moteurs à allumage commandé," PhD Thesis, 1997
33. Fontanesi, S., Cicalese, G., and Tiberi, A., "Combined In-cylinder / CHT Analyses for the Accurate Estimation of the Thermal Flow Field of a High Performance Engine for Sport Car Applications," SAE Technical Paper 2013-01-1088, 2013, doi:10.4271/2013-01-1088.
34. Fontanesi, S. and McAssey, E., "Experimental and Numerical Investigation of Conjugate Heat Transfer in a HSDI Diesel Engine Water Cooling Jacket," SAE Technical Paper 2009-01-0703, 2009, doi:10.4271/2009-01-0703
35. Malaguti, S., Fontanesi, S., Cantore, G., Montanaro, A., Allocca, L., "Modelling of Primary Breakup Process of a Gasoline Direct Engine Multi-Hole Spray," Atomization and Sprays, 23 (10): 861-888 (2013), ISSN Print: 1045-5110, ISSN Online: 1936-2684, 10.1615/AtomizSpr.2013005867.
36. Reitz, R., Diwakar, R., "Effect of Drop Breakup on Fuel Sprays," SAE Technical Paper 860469, 1986, doi:10.4271/860469.
37. Bai, C., Gosman, A., "Mathematical Modelling of Wall Films Formed by Impinging Sprays," SAE Technical Paper 960626, 1996, doi:10.4271/960626.
38. Colin, O., Benkenida, A., "The 3-Zones Extended Coherent Flame Model (ECFM3Z) for Computing Premixed/Diffusion Combustion," Oil & Gas Science and Technology – Rev. IFP, Vol. 59 (2004), No. 6, pp. 593-609.
39. Bruneaux, G., Poinsot, T., Ferziger, J.H. "Premixed flame–wall interaction in a turbulent channel flow: budget for the flame surface density evolution equation and modelling," Journal of Fluid Mechanics, 349, pp 191-219 doi:10.1017/S0022112097006769.

Definitions/Acronyms

B	Bore	τ_w	Wall shear stress
S	Stroke	**y**	Distance normal to the wall
SI	Spark Ignition	y_τ, y_τ^*	Characteristic length of the inner layer
DISI	Direct Injection Spark Ignition	y^+	Dimensionless distance
BMEP	Brake Mean Effective Pressure	v, v^*	Kinematic viscosity (local and mean of the inner zone)
°CA	Crank Angle Degree	v^+, v^{+*}	Dimensionless kinematic viscosity
aFTDC	After Firing Top Dead Center	v_w	Kinematic viscosity at the wall
bFTDC	Before Firing Top Dead Center	v_t	Eddy kinematic viscosity
BL	Boundary Layer	μ, μ^*	Dynamic viscosity (local and mean of the inner zone)
CHT	Conjugate Heat Transfer	μ_t	Eddy viscosity
TKE (k)	Turbulent kinetic energy	λ, λ^*	Thermal conductivity (local and mean of the inner zone)
RTD	Resistance Temperature Detector	λ_t	Eddy conductivity
θ^+, T^{+*}	Non-isothermal dimensionless temperature (i.e. dimensionless temperature for non-isothermal boundary layer)	Pr, Pr^*	Prandtl number

$\boldsymbol{\eta^+, y^{+*}}$	Non-isothermal dimensionless distance (i.e. dimensionless distance for non-isothermal boundary layer)	$\boldsymbol{Pr_t, Pr_t^*}$	Turbulent Prandtl number
$\boldsymbol{q_w}$	Wall heat flux	$\boldsymbol{\zeta}$	Isothermicity parameter
$\boldsymbol{\rho, \rho^*}$	Density (local and mean of the inner zone)	$\mathbf{p}$	Pressure
$\boldsymbol{\rho_w}$	Density at the wall	$\boldsymbol{\gamma}$	Ratio of specific heats
$\boldsymbol{\rho^+}$	Dimensionless density	$\boldsymbol{\dot{Q}_{comb}}$	In-cylinder gas-to-wall heat transfer
$\boldsymbol{c_p, c_p^*}$	Specific heat at constant pressure (local and mean of the inner zone)	$\boldsymbol{\dot{Q}_{fric}}$	Thermal power due to friction
$\boldsymbol{u_\tau, u_\tau^*}$	Friction velocity	$\boldsymbol{\dot{Q}_{surr}}$	Thermal power due to surrounding components
$\boldsymbol{T}$	Temperature	$\boldsymbol{\dot{Q}_{coolant}}$	Thermal power removed by coolant circuit
$\boldsymbol{T_w}$	Wall temperature	$\boldsymbol{\dot{Q}_{lubr}}$	Thermal power removed by lubricant circuit
$\boldsymbol{T_\tau, T_\tau^*}$	Characteristic temperature of the inner layer	$\boldsymbol{\dot{Q}_{env}}$	Thermal power lost to the environment
$\boldsymbol{T^+}$	Dimensionless temperature		

Appendix

Focusing the attention on the most diffused heat transfer models, they can be obtained from the mean energy conservation equation for the near-wall region under the following assumptions:

- fluid velocity is directed parallel to a flat wall and shear force is antiparallel to the flow direction;
- gradients normal to the wall are much greater than those parallel to the wall;
- pressure gradient is negligible;
- flow is quasi-steady;
- radiation is negligible;
- the gas is treated as ideal;
- Mach number is low (i.e. energy due to viscous dissipation is negligible);
- mass fractions of mixture components are constant near the walls;
- the effect of chemical reactions is negligible;

The mean energy conservation equation reduces to:

$$\frac{\partial}{\partial y}\left[(\lambda + \lambda_t)\frac{\partial T}{\partial y}\right] = 0 \qquad (11)$$

where λ and λ_t are the thermal conductivity and the eddy conductivity, respectively. Integrating the equation and introducing the Prandtl number ($= \mu c_p/\lambda$) and the turbulent Prandtl number ($= \mu_t c_p/\lambda_t$), the equation becomes:

$$-c_p\left(\frac{\mu}{Pr} + \frac{\mu_t}{Pr_t}\right)\frac{dT}{dy} = q_w \qquad (12)$$

At this point there are multiple choices to make the equation dimensionless, that is different kinds of distance/velocity/temperature scales can be used. Angelberger adopts the following ones:

$$u_\tau = \sqrt{\frac{\tau_w}{\rho_w}} \qquad T_\tau = \frac{q_w}{\rho_w \cdot c_p \cdot u_\tau} \qquad y_\tau = \frac{\nu_w}{u_\tau} \qquad (13)$$

obtained by means of wall quantities (such as wall density ρ_w and wall viscosity ν_w).

These scales are used to obtain non-dimensional wall distance (y^+) and temperature (T^+) respectively:

$$y^+ = \frac{y}{y_\tau} \qquad T^+ = \frac{T_w - T}{T_\tau} \qquad (14)$$

As a result, the dimensionless equation is

$$\left(\frac{1}{Pr} + \frac{\nu^+}{Pr_t}\right)\frac{dT^+}{dy^+} = \frac{1}{\rho^+}\frac{\nu_w}{\nu} \qquad (15)$$

with $\rho^+ = \rho/\rho_w$ and $\nu^+ = \nu_t/\nu$.

Now it is fundamental to distinguish among isothermal and non-isothermal flows:

- For ***isothermal*** (or quasi-isothermal) flows, ρ^+=1 and ν=ν_w so the equation simplifies and it becomes the same used by Kays and Crawford.

  $$\left(\frac{1}{Pr} + \frac{\nu^+}{Pr_t}\right)\frac{dT^+}{dy^+} = 1 \qquad (16)$$

  Therefore the law of the wall that can be obtained is valid for isothermal flows and is

  $$T^+ = 2.075 \cdot \ln(y^+) + 13.2 \cdot Pr - 5.34 \qquad (17)$$

  which, restricting considerations to air ($\sim Pr = 0.7$), becomes

  $$T^+ = 2.075 \cdot \ln(y^+) + 3.9 \qquad (18)$$

  and the heat flux results

  $$q_w = -\frac{\rho_w \cdot c_p \cdot u_\tau \cdot (T - T_w)}{T^+} \qquad (19)$$

  Equation (18) and (19) constitute the Kays and Crawford's heat transfer model.

- For ***non-isothermal*** flow $\rho \neq \rho_w$ (i.e. compressibility has to be taken into account) and $\nu \neq \nu_w$. Therefore, the equation does not simplify anymore. Angelberger identifies new variables

  $$d\eta^+ = \left(\frac{\nu_w}{\nu}\right) \cdot dy^+ \qquad d\vartheta^+ = \left(\frac{\rho}{\rho_w}\right) \cdot dT^+ \qquad (20)$$

  in order to let the equation become again similar to the Kays and Crawford one.

  $$\left(\frac{1}{Pr} + \frac{\nu^+}{Pr_t}\right)\frac{d\theta^+}{d\eta^+} = 1 \qquad (21)$$

  Angelberger assumes that all the considerations made by Kays and Crawford are still valid even if the flow is not isothermal; as a consequence, the non-isothermal law of the wall has the same form as the isothermal one proposed by Kays and Crawford, just with different variables accounting for the variation of gas properties (density and viscosity) with temperature:

  $$\theta^+ = 2.075 \cdot \ln(\eta^+) + 3.9 \qquad (22)$$

  Integrating $d\vartheta^+ = (\rho/\rho_w) \cdot dT^+$ the author is able to account for density variations within boundary layer in the expression of the heat flux,

  $$q_w = -\frac{\rho_w \cdot c_p \cdot u_\tau \cdot T_w \cdot ln\left(\frac{T}{T_w}\right)}{\theta^+} \qquad (23)$$

The last two expressions constitute the Angelberger's wall heat transfer model. From a practical point of view, comparing Angelberger's model with the Kays and Crawford's one, it is not pretentious to say that isothermal laws of the wall are applied to non-isothermal problems simply introducing new variables to redefine dimensionless distance and temperature.

It is worthwhile to note that the logarithmic expression of the dimensionless temperature (θ^+) is valid only for the inertial sublayer. As for the viscous sublayer, Angelberger adopts the simplified formulation $\theta^+ = Pr \cdot \eta^+$ (Figure 16). The switching point between the two expression of θ^+ is η^+_{sw} =13.2. Han and Reitz wall heat transfer model is very similar, since the expression of the heat flux (q_w) is the same and the logarithmic law of the wall changes its constants becoming:

$$\theta^+ = 2.1 \cdot \ln(\eta^+) + 2.5 \qquad (24)$$

Even if the wall function is very close to the Angelberger's one, Han and Reitz define it in a different way, including the effect of Prandtl number variations in the boundary layer.

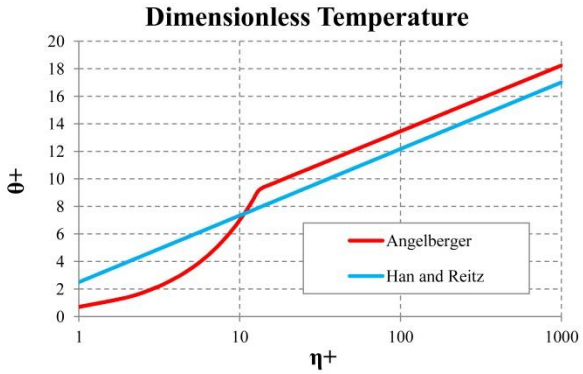

Figure 16. Dimensionless Temperature (θ^+): Angelberger and Han and Reitz formulations

As stated in the "Existing Model" paragraph, the main difference between the two heat transfer models is that Han and Reitz do not introduce the linear formulation for the viscous sublayer, as shown in Figure 16.